JOURNAL OF AIRCRAFT
Vol. 42, No. 1, January–February 2005

Large-Area Aerodynamic Control for High-Altitude Long-Endurance Sensor Platforms

Gregory W. Reich,* Jason C. Bowman,† and Brian Sanders‡
U.S. Air Force Research Laboratory, Wright–Patterson Air Force Base, Ohio 45433

The use of large-area aerodynamic control schemes to enable high-altitude long-endurance sensor platforms is investigated. The focus is on a vehicle with a joined-wing design. The vehicle has two performance shortcomings that are considered typical of the broader class of high-altitude long-endurance vehicles. The first is minimum roll rate at landing due to the large amount of roll damping associated with these configurations. It is shown that multiple distributed control surfaces can help meet the roll rate requirements. The second is sensitivity of takeoff gross weight to maximum lift-to-drag ratio. Notional mission requirements drive the fuel fraction to high levels and small changes in lift-to-drag ratio can enable large changes in the vehicle weight through reduced fuel requirements. It is shown that the same technology used to satisfy the roll requirement can also be used to actively control the twist and camber during cruise and can have a moderate impact on the vehicle weight or endurance.

I. Introduction

THE U.S. Air Force (U.S.A.F) has great interest in developing unmanned intelligence, surveillance, and reconnaissance (ISR) platforms in pursuit of Information Dominance. This is demonstrated by the increased use of high-altitude long-endurance (HALE) systems such as the Predator and Global Hawk, which are unmanned ISR platforms currently operated by the U.S.A.F. New research efforts are targeting higher density sensor platforms for information gathering with much larger ranges and endurance, and a few critical technologies have been identified as major enablers for such systems. One of the top priorities is active aerodynamic control. This can be accomplished through either flow control, such as surface roughness, or shape control, such as camber and twist variations. In this paper we focus on the latter technique.

A number of suitable shape control technologies have already been demonstrated for potential HALE vehicle applications. The Mission Adaptive Wing (MAW) program investigated the use of smoothly varying leading- and trailing-edge camber over three spanwise segments on an F-111 aircraft.[1] Improvements in several metrics were demonstrated, one of which was enhanced maneuver performance. For example, a 25% increase in roll performance was demonstrated during flight test. Cruise performance was also greatly improved due to the ability to tailor the shape of the supercritical airfoil, reflected in range increases of 28% in some mission segments. Finally, the research program demonstrated that, just as the spanwise load can be varied to reduce drag in cruise, it could also be utilized for load alleviation.

Another applicable technology to emerge is active aeroelastic wing (AAW) technology.[2] AAW technology provides a method to control aerodynamic shape through a combination of leading-edge and trailing-edge control surfaces and wing twist. The energy to drive this system comes from a combination of mechanical actuators and aerodynamic work. It has been demonstrated that high control authority is maintained up to low supersonic conditions. This increase is obtainable while maintaining a fair amount of wing flexibility. This capability translates directly into reducing wing weight.

Advancements in mechanism and actuator design have the potential to further improve the MAW and AAW concepts. One of these is the technology developed under the Smart Wing project.[3] This project demonstrated the use of high-speed ultrasonic piezoelectric motors to drive a series of connected control surfaces. This system of surfaces provided for a smoothly varying deformation of the control surface (similar to MAW) and a smoothly varying spanwise variation. A deflection of 25 deg at 70 deg/s was demonstrated in the wind tunnel. Some new mechanical design concepts[4,5] are also starting to mature that will further integrate mechanism and structures and lead to enable shape control. One technology is the compliant mechanism approach that Lu and Kota[4] have demonstrated for conformal leading-edge and trailing-edge control surfaces. Also of note are piezoceramic fiber composites[6,7] that allow direct actuation of structure with embedded actuator systems. The goal of this study is to demonstrate how the aerodynamic benefits made possible by these technologies can be utilized into the design of a HALE vehicle and enable it to meet mission requirements.

II. Sensorcraft Concept, Design Requirements, and Mission Objectives

In pursuit of the next generation of ISR platforms, the Air Force Research Laboratory (AFRL) conducted a technology assessment study[8] of a HALE vehicle called Sensorcraft. The goal of the study was not to produce a vehicle design for transition into preliminary and detailed design. Rather, it was to determine the technologies that may be required to make such a vehicle viable. This meant producing a vehicle design with the required fidelity to evaluate technologies for their effect on the overall vehicle performance.

The notional mission for this design is shown in Fig. 1. This mission has approximately a 150% increase in range and 67% increase in time on station compared to Global Hawk. In the assessment study, emphasis was placed on antenna performance and requirements over traditional vehicle performance requirements. The most important performance metric for the vehicle to meet was 360-deg radar coverage. Of the few possible configurations that met this requirement, a joined-wing design with dual, offset fuselages was selected. (For other joined-wing analysis and design studies, see work such as those by Blair and Canfield[9] or Wolkovitch.[10]) Both vhf (a long wire) and x-band (flat phased-array panels) antennas were to be carried, as shown in Fig. 2. The phased arrays were mounted on the front face of the wing structural box on the forward wings and on the rear face of the wing box on the rear wings. Because of potential interference with the antennas, control surfaces

Received 18 December 2003; revision received 1 April 2004; accepted for publication 1 April 2004.

*Research Aerospace Engineer, Air Vehicles Directorate, AFRL/VASA, 2210 8th Street, Room 219. Senior Member AIAA.
†Research Aerospace Engineer, Air Vehicles Directorate, AFRL/VASA, 2210 8th Street, Room 219.
‡Senior Research Engineer, Air Vehicles Directorate, AFRL/VASA, 2210 8th Street, Room 219. Associate Fellow AIAA.

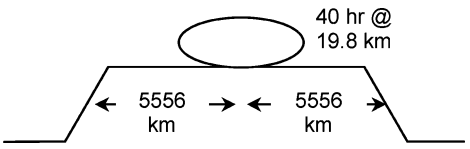

Fig. 1 Basic sensorcraft mission.

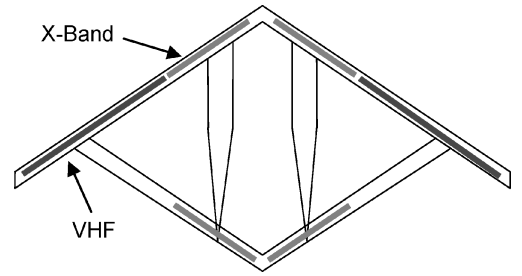

a)

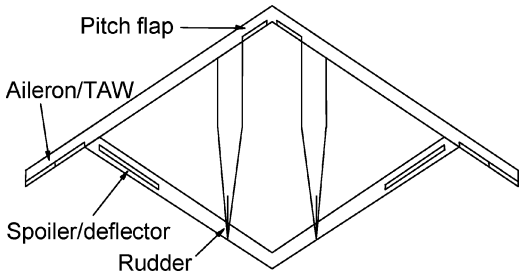

b)

Fig. 2 AFRL sensorcraft technology assessment model: a) antenna placement and b) control surface placement.

were limited to the leading edge on the rear wings and the trailing edge on the forward wings. The layout of the control surfaces is also shown in Fig. 2.

The resultant vehicle design was able to meet all of the stringent performance requirements. However, the design was not robust to any variations in the design. It existed near several regions of infeasibility—aerodynamic, flying qualities, propulsive, and structural, and any small variation would make it infeasible. Because the vehicle design is balanced on the pinnacle of a very steep design surface, for example, a small change in the a design parameter will have a large impact on final vehicle design, it is possible that active aerodynamic control could assist in making the vehicle design more robust to design changes, as well as to improve the performance of the vehicle in key mission segments.

There are two mission segments where this technology could potentially have an impact on the Sensorcraft performance. The first is the landing phase because the current vehicle configuration is unable to meet a roll rate requirement at landing. The wing configuration that satisfies both the antenna and cruise requirements has an unusually high roll damping (approximately 50% higher than a typical value for a transport class aircraft) due to the large aspect ratio. With the wing highly cambered for loiter, the landing speed at 40% takeoff gross weight (TOGW) that allows the vehicle to land in a trimmed, nose-up attitude does not generate enough dynamic pressure to produce a rolling moment high enough to meet the roll requirement. Landing at an airspeed that meets the roll requirement results in a trimmed, nose-down landing attitude. Although not a crash, landing nose first introduces yaw stability problems on roll out, not to mention requiring a heavy nose gear. However, if the wing can be uncambered for landing, the vehicle can land at higher speeds in a nose-up attitude.

The second mission segment for potential use of variable camber is the loiter phase. To achieve 360-deg coverage, the wing sweep angles must exceed a certain minimum, with 45 deg being ideal for sensor performance. Without increasing wing span, which is difficult due to the flexible nature of this configuration, the restrictions on sweep limit the maximum lift-to-drag ratio L/D. As configured, an estimate based on similar HALE aircraft yields a maximum L/D of about 30. It was shown during the initial technology assessment that if a 30% increase in L/D could be achieved, the gross weight would decrease from approximately 32,000 to 13,500 kg. One approach to achieve this increase is to use active flow control to improve the aerodynamic efficiency over the entire mission spectrum. Another is to continuously vary the camber in-flight to better match the geometry to the current altitude, speed, and weight while still satisfying antenna requirements.

The remainder of this paper addresses the application of structural shape control for aerodynamic performance to the conceptual Sensorcraft vehicle. In the next section, two separate technologies, variable camber and wing twist, are studied for their ability to meet a minimum roll rate during the landing segment of the mission. The following section addresses increasing mission endurance or decreasing vehicle weight through optimal airfoil shape control across the loiter segment.

III. Roll During Landing

As discussed earlier, it appears that large-area, distributed aerodynamic control can have a significant affect on the roll requirement at landing. For this application, we address landing because it is more critical than takeoff. The vehicle is approximately twice as heavy at takeoff as at landing, requiring twice the dynamic pressure to become airborne. Although the roll inertia is higher at takeoff, the relatively higher takeoff speed produces rolling moments roughly 100% higher than landing but roll inertias only about 15% higher. The solution to this problem is inhibited by the limited allowable placement of control surfaces, except for the most outboard sections of the wing. Inboard (of the joint) control surfaces may not be effective because the downwash on the rear wing negates the increase in lift on the forward wing caused by the deflection of a control surface. This effect may be only apparent near the wing joint, where the two wings are in close proximity to each other.

Two solutions were investigated in this study. The first is large-scale twist of the outer wing panel, which may be possible with the use of piezoceramic fiber composites. The second is AAW technology. Large-scale twist of the outer section is an attractive solution because it would not hinder the performance of the antennas. AAW technology is attractive because it involves numerous smaller control surfaces working in coordination with each other. It can also have other system benefits such as drag reduction and gust load alleviation.

To investigate these potential solutions, an aeroelastic model was used for a roll trim analysis of the Sensorcraft vehicle. The simplified aeroelastic model used in this study is a beam-rod version of the Sensorcraft structural model.[11] This model, shown in Fig. 3, preserves the mass and inertia properties of the full model and consolidates the stiffness properties of each wing onto a single beam. The associated aerodynamic model is a ZAERO panel model as implemented in a version of ASTROS.[12,13] Not shown in Fig. 3 is the jig shape of the aerodynamic planform, which is a nonlinear twist distribution from positive angles on the inboard wing to a negative angle at the tip. The aft wing jig shape is also a non-linear twist distribution of positive angles.

The aeroelastic analysis of the roll control problem during landing is limited to quasi-static trim solutions at single points of time. Trim solutions for a rigid or flexible vehicle can be found for any combination of roll acceleration, roll rate, and control surface deflections. Although not manned, it was decided to apply the roll requirement for manned vehicles because the requirements have yet to be defined for unmanned vehicles. For transportlike aircraft, the requirement is to roll 30 deg in 2.5 s. The initial roll acceleration or steady-state roll rate to meet this requirement can be determined for a rigid vehicle from the solution of the dynamic equation for roll,[14] which is

$$I_x \dot{p} = [C_{l_p}(pb/2V) + C_{l_\delta}\delta]qSb \tag{1}$$

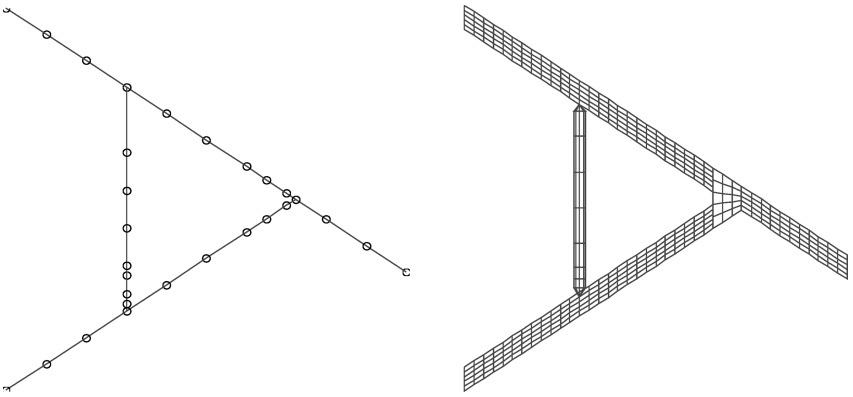

Fig. 3 Sensorcraft structural and aerodynamic models.

where I_x is the vehicle moment of inertia about the longitudinal axis, $\dot{p}$ is the roll acceleration, C_{l_p} is the coefficient of rolling moment due to roll damping, C_{l_δ} is the coefficient of rolling moment due to a control surface deflection, δ is the control surface deflection, p is the roll rate, b is the total wing span, V is the freestream velocity, q is the dynamic pressure, and S is the wing area. For a step control input, the roll angle at time T is given by

$$\phi(T) = p_\infty\{T + \tau[\exp(-T/\tau) - 1]\} \tag{2}$$

where p_∞ is the steady-state roll rate and $\tau = -(1/L_p)$ where $L_p = (qSb/I_x)(b/2V)$. The initial roll acceleration required is then

$$\dot{p}(0) = (qSb/I)C_{l_\delta} \tag{3}$$

and, alternatively, the steady roll rate required is

$$p_\infty = \left(C_l/C_{l_p}\right)[1/(b/2V)] \tag{4}$$

The solution methodology for Eq. (3) or (4) is to determine the unknown control surface deflections δ based on a given roll rate or acceleration. For the general case where there are several control surfaces, this equation is insufficient to uniquely determine a combination of control surfaces that satisfies the trim equation. Therefore, an optimization process is required to add sufficient constraints to the problem so that a solution is possible.[15,16] The objective function for this optimization process could come from a number of sources, such as minimizing the total control surface deflections, minimizing the structural deformations, or minimizing the work or energy required to deflect the surfaces and create the required roll. Constraints for the trim optimization problem are typically defined as limits on maximum control surface deflection, satisfaction of the trim balance equation, and, for conventional control surfaces, a maximum hinge moment above which the control surface actuator lacks the authority to deflect the control surface the desired amount.

A. Twist Actuation

A first step toward resolving the roll problem on landing is to determine whether outboard twist alone is sufficient to meet the roll requirement. To determine this, the outboard section of the wing is defined as a series of 11 independent control surfaces running from leading to trailing edge, as shown in Fig. 4, all hinged at the wing structural beam location. The sensitivity of roll with respect to each aerodynamic control surface can be determined, and this information used to determine an optimum twist distribution to meet the roll requirement. This approach is a modeling approximation to embedded piezoceramic fiber composites and can be considered as an upper bound on the roll performance. Any structural actuator would have lower performance simply because this approach has no stiffness in twisting the structure. The aeroelastic model does have splining to transfer aerodynamic loads to the structural model and structural displacements to the aerodynamic model. However, the deflection of a control surface is not directly tied to the stiffness of the structure, so that the forces required to deform the structure are not considered.

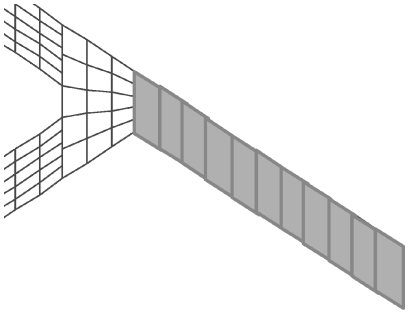

Fig. 4 Outboard twist actuators for roll study.

To determine if twisting the outboard wing is sufficient to meet the roll requirement, a trim optimization is done to determine control surface displacements needed to trim the vehicle for initial required roll acceleration at low speed. A steady-state roll rate of 0.226 rad/s, determined from Eq. (4), is used as a target for the Sensorcraft vehicle at $M = 0.15$, 10% fuel load on landing. The optimization to be solved is a minimization of the total hinge moment or aerodynamic work of the system. That is, for each control surface, the amount of work done to overcome the hinge moment and deflect the surface to the given deflection angle is computed. This value is summed over all of the surfaces, and the function is minimized subject to the vehicle trim balance and deflection limits. The aerodynamic work is defined as

$$M_h = \sum_i \frac{1}{2}\frac{\partial M_{hi}}{\partial \delta_i}\delta_i^2 \tag{5}$$

where i represents the summation over all control surfaces. For this particular case, there is no true hinge moment for each control surface because the structural actuators are generating a twist of the structure itself. However, we can compute an equivalent aerodynamic moment that represents the moment required to overcome the aerodynamic loads and twist that portion of the structure to the required levels.

The result of the trim optimization study is that the minimum twist angle solution deflects all of the control surfaces approximately 24 deg. This value is extremely large for structural twist and is probably too large to be achieved effectively. Additionally, the aerodynamic moments developed by the control surfaces at these twist angles are on the order of 150 N · m. Even if the structure could be designed such that the structural moments of inertia were small enough so that this twist level was achievable, it is highly doubtful that a twist actuator would be able to overcome both the aerodynamic and structural moments opposing the twist.

Alternatively, Eq. (1) can also be solved for a roll rate given a set of maximum control surface deflections, which provides an indication of the maximum roll rate that could be met. For a twist deflection limit of 10 deg, that roll rate is 0.091 rad/s, or about half the

required rate for landing. For a limit of 5 deg, the rate is 0.046 rad/s. These results are similar to those found by Cesnik and Brown[7] for a similar HALE vehicle study using embedded twist actuation over the outboard section of a wing. For both of these situations, the aerodynamic hinge moment is still on the order of 150 N · m. This is because the hinge moment in this case is generated for the most part by the rolling motion. Clearly, twist actuation on the outboard wing section is not adequate for the roll on landing problem.

B. AAW Technology

As an alternative to twist actuation, a different control surface scheme is investigated, one that utilizes a number of leading- and trailing-edge control surfaces spread across the aerodynamic planform. One possible scheme is the layout in Fig. 5. This layout, applied to the Sensorcraft vehicle to investigate minimization of structural deformations,[11] is based on AAW technology.[2] As already mentioned, the outside of the diamond planform is off limits to control surfaces due to the antenna requirements. Therefore, the inside of the diamond is populated with control surfaces, as well as the leading and trailing edges of the wing outside of the joint.

Table 1 contains data and results from this control scheme for rolling the Sensorcraft. In the second column, the rolling moment coefficients for each control surface are given. As was anticipated, the outboard trailing edge surfaces 4 and 6 have the largest effect on roll and are, therefore, utilized to their full extent. Additionally, the leading-edge control surfaces have a much smaller effect on roll at low speeds. This result is expected because it is well known that leading-edge control surfaces have very little effect except at higher speeds. The optimization process produces the solution shown in the third column of Table 1. For this solution, surface 4 is used to its full extent, as are surfaces 3 and 6. In fact, the rolling requirement is so large that the minimum deflection for surface 4, assuming full 30-deg deflections on all five other surfaces, is approximately 23.5 deg.

The hinge moments for this solution are given in the fourth column of Table 1. The hinge moments range in magnitude from 257 N · m down to almost zero for surface 5, indicating that this surface is for all intents and purposes unloaded. This means that at this trim condition, very little actuation force is required to hold the control surface at that deflection angle. Note that the aeroelastic model for the structure and control surfaces does not contain any stiffness in the control surface hinges themselves, and therefore, all of the energy required to hold a control surface at a particular deflection level must come from the actuator.

It is interesting to see just how these values for hinge moment are developed. The last column of Table 1 shows the contribution to the hinge moment from the rolling motion itself. That is, this is the value of hinge moment that would be measured on a control surface at the steady-state roll rate of 0.226 rad/s without any deflection of the control surface. Generally, the roll motion contribution to the aerodynamic forces should be linearly increasing out the span and downward (against the rolling direction). If that is so, the hinge axis locations are such that the leading-edge control surfaces see a negative hinge moment due to roll and the trailing edge surfaces see a positive hinge moment. The last column of Table 1 reflects this: The hinge moments due to roll are negative for the leading-edge surfaces and positive for the trailing edge. However, the values are not increasing out the span on the leading edge. Although the change in local angle of attack due to roll is linear out the wing, the resultant local lift distribution is not.

Table 1 Control surface deflections and hinge moments for AAW trim solution

Control surface	C_{l_δ}, rad^{-1}	Deflection, deg	Hinge moment, N · m	Hinge moment due to roll only, N · m
1	0.0011	−3.31	256.9	−95.9
2	0.0073	14.38	−15.3	−50.7
3	0.0131	30.00	−160.1	−98.8
4	0.1301	30.00	241.7	143.9
5	0.0251	1.33	0.1	1.8
6	0.0658	30.00	12.3	35.4

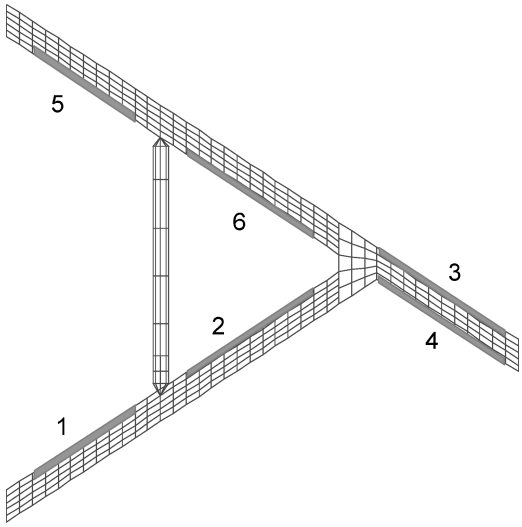

Fig. 5 Sensorcraft AAW control surface layout.

C. Subdivided AAW

The control surfaces in the AAW scheme are either 6.1 or 7.6 m wide (spanwise) and either 2.4 or 3.2 m^2 in area (covering 20% of the chord length), quite large surfaces for individual actuators to handle. Instead of adding actuators to reduce the load on each actuator, these surfaces can be subdivided, decreasing the area and, therefore, the hinge moment on each actuator. To investigate the behavior of the system with smaller surfaces, the control surfaces in Fig. 5 were divided into four or five sections, and the trim optimization was rerun. Each of the 28 control surfaces was 1.5 m wide and had an area of 0.65 m^2 (with the same 20% chord length).

The result from this analysis appears in Table 2. As expected, the hinge moments on each surface have been reduced due to the smaller size of the control surfaces. More interesting, though, is the action of the optimizer and how it has chosen to utilize the smaller surfaces. In some places, such as control surfaces 4 and 6, the subdivided solution mimics the original solution in that all of the smaller surfaces have the same displacement as the larger one did. However, surfaces 2 and 5 leave some smaller surfaces undeflected, whereas others are deflected to the maximum amount. The original solution, with less refinement, is forced to choose a value between the two extremes. Generally, the more redundant control surfaces there are, the more load control, wing shaping, and other secondary activities can be achieved while still meeting the primary purpose of the control surfaces—controlling and trimming the vehicle.

Table 2 Control surface deflections and hinge moments for subdivided AAW trim solution[a]

Control surface	Deflection, deg	Hinge moment, N · m	Control surface	Deflection, deg	Hinge moment, N · m
1a	1.08	43.7	4a	30.00	30.0
1b	1.33	100.7	4b	30.00	38.8
1c	0.42	106.1	4c	30.00	38.1
1d	0.79	105.2	4d	30.00	38.8
2a	0.00	−7.4	4e	30.00	29.6
2b	30.00	−1.3	5a	0.00	−0.6
2c	30.00	−4.2	5b	0.00	0.3
2d	17.45	−7.3	5c	0.00	0.4
2e	30.00	−9.9	5d	30.00	−0.4
3a	30.00	−30.8	6a	30.00	0.5
3b	26.72	−46.1	6b	30.00	2.0
3c	26.20	−50.9	6c	30.00	2.8
3d	30.00	−47.7	6d	30.00	0.2
3e	30.00	−50.0	6e	30.00	−18.7

[a]Subdivided surfaces listed from inboard to outboard on each larger surface.

Another interesting observation about Table 2 is that the hinge moments on a control surface group also do not always match the trends from the earlier case in Table 1. The biggest example of this is on surface 6. The control surface deflections do match those from Table 1, but the hinge moments do not. Surface 6e has a negative hinge moment, as opposed to the positive hinge moment on surface 6 from Table 1 and surfaces 6a–6d in Table 2. This may be due to the proximity of this surface to the rear wing and the wing joint, both of which could have a significant affect on the aerodynamic response.

D. Massively Subdivided AAW

One desirable feature of a seamless, smoothly contoured wing is that it has a low radar cross section. Gaps between control surfaces edges represent significant increases in radar cross section and increase the drag due to three-dimensional effects around the control surface edges. These gaps occur where two adjacent control surfaces have very different deflection values, such as between surfaces 2a and 2b in Table 2. Therefore, it is desirable to attempt to smooth out the spanwise variation in control surface deflection as much as possible. In the limit, the control surfaces could be implemented as continuously variable surfaces with a flexible skin of some kind filling the gaps between surfaces, such as those demonstrated with continuous moldline technology[17] or on the Smart Wing.[3]

To address this concern, and to demonstrate how far the subdivided AAW approach can be pushed, a final analysis was run using subdivided control surfaces with spans of approximately 30 cm and the same chord length. At this point, the discretization of the original control surface has progressed to the point that it approaches a smoothly varying contoured control surface. To achieve this, a new aerodynamic paneling was required, one with greater refinement to model all 140 of the 0.12-m^2 control surfaces. This panel model, shown in Fig. 6, has increased spanwise refinement across the entire planform and increased chordwise refinement around the hinge lines of the control surfaces.

In addition to increasing the number of subdivided control surfaces, an additional constraint was added to the trim optimization routine to enforce smoothness on the spanwise variation. This constraint prohibits adjacent control surfaces from having widely divergent deflections, demonstrating the feasibility of creating truly smooth contours on the control surfaces. The constraint is defined as

$$|\delta_i - \delta_{i-1}| < \varepsilon \tag{6}$$

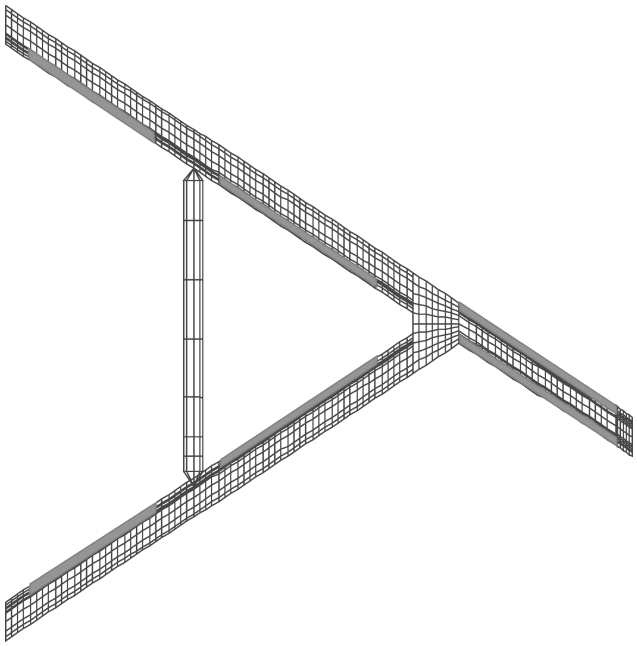

Fig. 6 Refined aerodynamic panel model for massively subdivided AAW solution.

where ε is a predetermined tolerance. Note that, in this analysis, the control surfaces cannot twist, and so the spanwise shape of the control surface is stepped. As the number of control surfaces increases, and the size of each surface decreases, this scheme approaches the smoothness demonstrated by the Smart Wing model,[3] where each control surface could both deflect and twist, creating a spanwise slope and increasing the smoothness of the control surface shape.

The results of this analysis are shown in Fig. 7. The smoothness constraint of Eq. (6) uses a limit of $\varepsilon = 5.0$ deg. Clearly, the smoothing constraint is active, forcing the control surfaces into shapes similar to those demonstrated on the Smart Wing.[3] As expected, the outboard trailing-edge surfaces (4 and 6) are the most utilized. However, note the behavior of control surface 2, the outer of the leading-edge surfaces on the aft wing. The trim solution has two bumps of nonzero deflection on this surface. These do not correspond to regions of higher C_{l_δ}, nor do they reflect trends apparent in the earlier sections. They are artifacts of the optimization procedure, attempting to minimize the aerodynamic work during trim. Although not reported, the hinge moment values are predictably small compared to those in the preceding solutions due to the smaller size of the control surfaces.

The important point to remember from the AAW solutions is that camber variation (as represented by deflection of a control surface) can be effective in meeting the required roll control for landing. Therefore, we will focus on combinations of twist and camber that meet performance requirements throughout the mission profile. Specifically, the remainder of this paper addresses the determination of twist and camber profiles to decrease fuel consumption in cruise and loiter leading to lower gross weight or extended loiter times. These shapes can be used in the future as performance objectives for an adaptive wing shaping system.

IV. Cruise and Loiter Performance

The loiter segment for Sensorcraft is unusually long, requiring a very high fuel fraction. The typical wing aerodynamic design procedure is to select the camber and twist distribution at the average lift coefficient that not only produces the minimum amount of induced drag but also trims the vehicle. At other lift coefficients, a control surface is deflected to trim the vehicle. Not only does a deflected control surface increase the pressure drag, but it also alters the total spanwise lift distribution and flow over any surfaces aft, thereby increasing induced drag. With an adaptive structure, it becomes possible to command the optimal shape throughout the mission. In both the landing and loiter phases, the same mechanism can be used because either solution depends on changing wing camber and twist.

A. Sensitivities

Adaptive structures can be used to reduce the fuel required in cruise and loiter for Sensorcraft by optimizing the wing throughout the mission. Sensorcraft is especially sensitive to small changes in maximum L/D, which is a primary indicator of fuel consumption. To understand this sensitivity, consider the total vehicle weight, calculated as

$$W_{\text{TO}} = W_{\text{payload}}/(1 - W_{\text{fuel}}/W_{\text{TO}} - W_{\text{empty}}/W_{\text{TO}}) = \text{GF} \times W_{\text{payload}} \tag{7}$$

where $W_{\text{fuel}}/W_{\text{TO}}$ and $W_{\text{empty}}/W_{\text{TO}}$ are the fuel and empty weight fractions.[18] When these weight fractions are high enough to make the denominator close to zero [large growth factor (GF)], the vehicle weight becomes extremely sensitive to parameters that affect fuel and empty weight, such as engine and aerodynamic efficiency. An estimated maximum L/D of 30 was assumed, and the specific fuel consumption that achieved the nominal loiter using the standard Breguet equations was computed at approximately 0.4 N (fuel/h/N) thrust. Note that a turbofan engine with this efficiency does not yet exist. The sensitivity of gross weight to L/D can be obtained by computing the derivative $(\partial W_{\text{TO}}/W_{\text{TO}})/(\partial L/D/L/D)$.

The results are shown in Fig. 8, with the baseline vehicle indicated with an asterisk. Figure 8a shows the changes in maximum lift-to-drag ratio, whereas Fig. 8b shows the sensitivity of takeoff weight

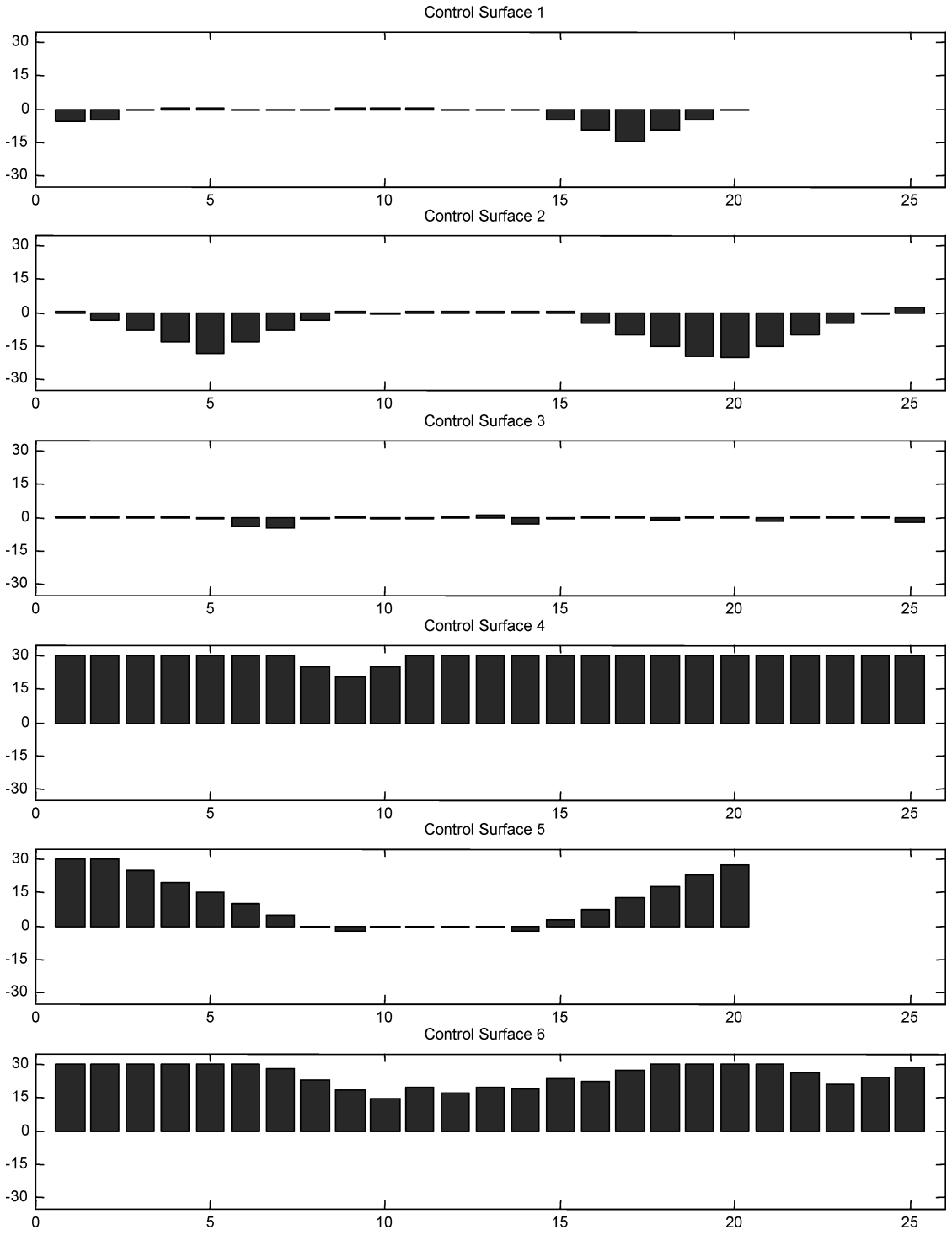

Fig. 7 Control surface deflections with smoothness constraint of 5 deg.

to changes in the maximum lift-to-drag ratio. For small changes, the sensitivity term can be thought of as the ratio of percent change in takeoff weight to the percent change in L/D. Therefore, a 1% increase in average L/D on the baseline vehicle would result in approximately a 6% decrease in TOGW. The sensitivity of TOGW with respect to L/D is unusually high due to the lengthy loiter requirement (large fuel fraction, which causes GF to be large).

Lift-to-drag ratio can be improved through flow control, which affects parasite drag, or shape changes, which can affect parasite and induced drag. Shape changes can affect, in approximate descending order of magnitude for the baseline vehicle, primary induced drag (excluding trim and span effects), reducing wetted (exposed) area, increasing span, decreasing sweep, lowering trim drag, and increasing span efficiency. Because large planform changes are not possible, the feasible choices become flow control and airfoil shape changes to reduce induced drag, trim drag, and span efficiency.

The main induced drag effect can be seen in Eq. (8). The C_{L_0} term mostly depends on camber, twist, wing incidence relative to the fuselage, and to a lesser extent the fuselage shape. If the flight lift coefficient is very different than C_{L_0}, the induced drag can be excessive due to the quadratic dependency on lift coefficient,

$$C_D = C_{D_p} + k\left(C_L - C_{L_0}\right)^2 \tag{8}$$

Trim drag is the additional induced drag caused by a deflected control surface used for trim. Span efficiency is the ratio of induced drag to the minimum realizable induced drag at the same lift coefficient. Span efficiency is a function of chord, camber, and twist distributions as well as Mach number and lift coefficient. Only the

elliptic wing with no twist achieves 100% efficiency for any subsonic Mach number and lift coefficient.

Because wings are typically shaped (cambered and twisted) and trimmed with no control deflection for the midmission condition, operating off this condition for extended periods can have a noticeable effect on fuel required due to primary induced drag, trim drag, and span efficiency. For a constant speed, constant altitude profile, the lift coefficient varies from approximately 1.1 at the start of the mission to 0.4 at the end. This is a significant variation from a design point of, for example, $C_L = 0.75$.

B. Twist and Camber Design

To investigate the weight and performance improvements possible in cruise and loiter through the addition of large area aerodynamic control using adaptive structures, an analysis is done to find the optimal vehicle twist and camber distributions at various points throughout the mission. It is assumed that a suitable adaptive structure capable of assuming these shapes exists, such as those discussed earlier. Sensor power requirements are already factored into the fuel consumption, but actuation power is not. It is assumed that a feasible actuation system for primary shape control will have a low duty cycle (off and mechanically locked when not in operation) and not contribute to the fuel consumption.

The mission profile chosen is a constant altitude, constant Mach number cruise and loiter, which is the least efficient profile. The results shown in Fig. 8 are based on a cruise–climb, the most efficient profile. If the vehicle can cruise–climb, then there is little reason to adapt the wing geometry because the lift coefficient is constant, except possibly for vehicle control with a flexible structure. The other mission profile, a constant altitude, decreasing Mach number loiter, which also maximizes L/D, is not realistic because the statistical winds aloft would force the vehicle off station.

The design process begins by taking the planform geometry and applying the methods in the NASA report by Lamar,[19] referred to as the design code. The result is a set of camberlines that achieve the specified lift coefficient at the desired Mach number with minimum induced drag such that the vehicle is trimmed. The analysis process begins by transferring the camberlines to HASC, a vortex lattice aerodynamic code used for computing lift, drag, and moment coefficients.[20] No modifications are made for the adaptive vehicle. However, the induced drag calculated by HASC is used to have a fair comparison with the nonadaptive vehicle, which has to be trimmed in HASC because the design code cannot do analysis. For the nonadaptive vehicle, this design process is accomplished at a design lift coefficient of 0.75. The HASC geometry is modified to include a pitch flap for the first 3 m of semispan on the forward wing, using the entire chord as the control surface. A trim loop is then used to find the trimmed control surface deflection and, more important, the induced drag for each trimmed lift coefficient. This process is repeated for static margins from −5 to 120% (center-of-gravity locations ranging from 13.7 to 16.7 m from the leading edge of the forward wing root). Implicit in this induced drag calculation are the primary induced drag effect $(C_L - C_{L_0})^2$, trim drag, and span efficiency.

The results show an approximate improvement in induced drag coefficient of 0.002 over the entire lift coefficient and static margin range. Figure 9 shows the resultant wing twist and camber with positive static margin as fuel is burned. From Fig. 9a, the front wing demonstrates changes in twist (twist curves converge) and camber, and the rear wing demonstrates mostly a change in incidence (twist curves are parallel). This is consistent with a conventional wing and tail. The camber change is mostly at the trailing edge and has a smooth spanwise distribution. (If a structural model were coupled with the aerodynamic model, changes in the leading edge camber might be observed as well as they were in the roll problem.) This suggests that a technology such as that demonstrated in the Smart Wing program could be applied to achieve this distribution.

The improvement in induced drag, 0.002, appears lower than what might be expected and could be a result of several factors. For one, the span efficiency is already high due to the high aspect ratio, and therefore, the level of possible improvement is smaller than expected. Additionally, the operating lift coefficients may be high compared to the minimum drag lift coefficient C_{L_0} even with optimized twist and camber. This means that the basic induced drag effect $(C_L - C_{L_0})^2$, may be dominating the results.

Another issue that has an unknown effect on the results is the disagreement between the design and analysis codes. The induced drag was in good agreement, but the pitching moments demonstrated a relatively high bias with angle of attack. To deal with the issue, the pitching moment that HASC reported at the midmission lift

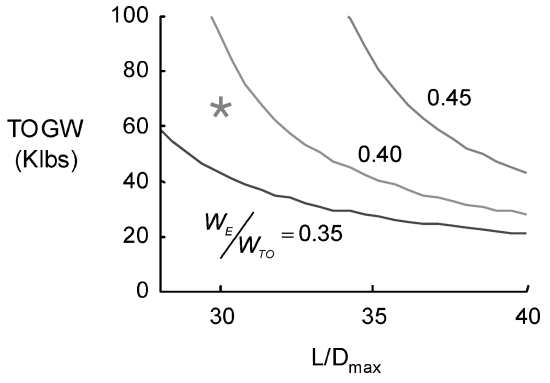

Fig. 8a Takeoff weight vs maximum lift-to-drag ratio.

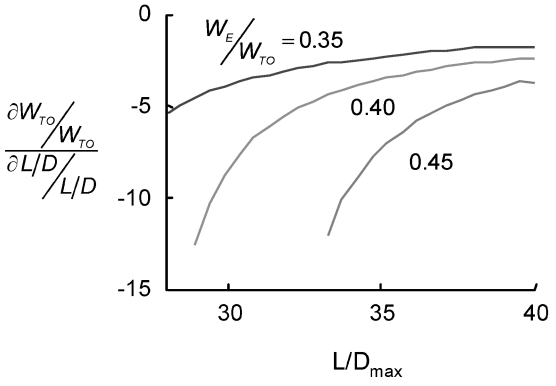

Fig. 8b Sensitivity of takeoff weight to changes in maximum lift-to-drag ratio.

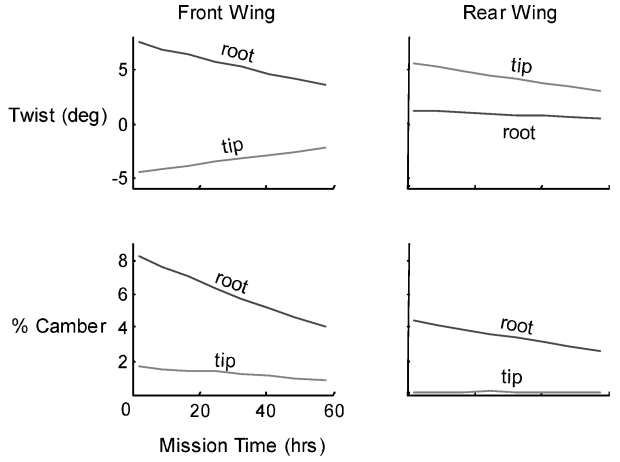

Fig. 9a Wing geometry changes throughout the mission.

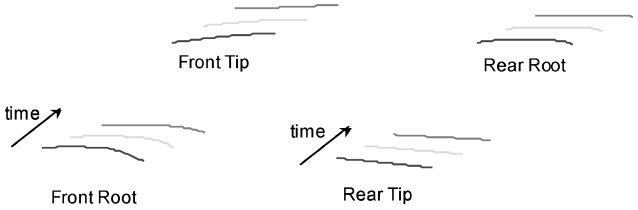

Fig. 9b Root and tip mean surfaces at the start, middle, and end of cruise.

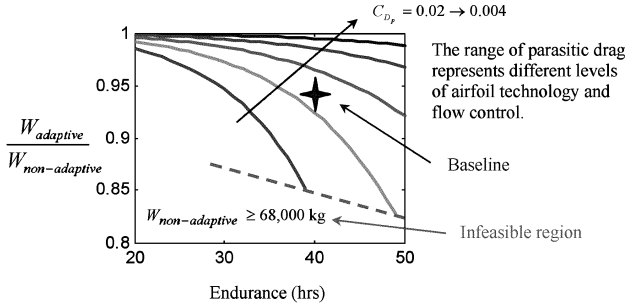

Fig. 10a Relative weights of adaptive and nonadaptive vehicles as a function of endurance.

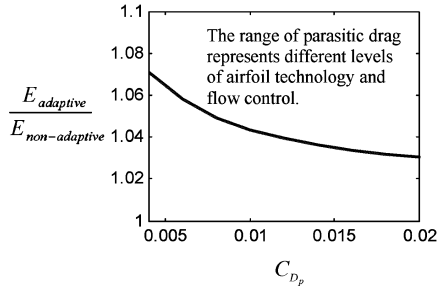

Fig. 10b Relative endurance of adaptive and nonadaptive vehicles for the same weight.

coefficient, and not zero pitching moment, was used as the trim point at other lift coefficients. Whereas this approach works at the design lift coefficient, it is not certain if the approach is valid at the off-design conditions.

The final step is to form a complete drag polar by assuming a parasitic drag coefficient. A simple drag buildup assuming fully turbulent flow yields a $C_{D_p} \approx 0.015$. Assuming fully laminar flow, $C_{D_p} \approx 0.003$. For the higher parasitic drag values, the improvement in lift-to-drag ratio is about 6% at the extreme off-design lift coefficients. The average L/D improvement is obviously lower and must be estimated by integrating the fuel flow over the entire mission.

The improvement in L/D can be used in two different ways. The first is to reduce the gross weight for the same mission requirements. The second is to increase the endurance for the same fuel and gross weight as the baseline vehicle. Figure 10a shows the reduction in gross weight for the same mission over the range of parasitic drag coefficients discussed earlier. The results demonstrate a maximum gross weight savings of 15% with about 5% at the baseline endurance requirement. The savings are smaller for lower parasitic drag, for example, flow control, because the basic lift-to-drag ratio is then high enough to place the design in a lower sensitivity portion of the design space. The savings are larger for higher parasitic drag, but even the adaptive vehicle weight is excessive. [The plot (Fig. 10a) is cutoff where the nonadaptive vehicle mass exceeds 68,000 kg.] Figure 10b shows the change in endurance possible for the same gross weight and fuel. Using the improvement in lift-to-drag ratio to fly longer for the same fuel yields approximately 7% improvement for fully laminar flow, 3.5% for fully turbulent flow, and 4.5% at the baseline.

The results are not spectacular with a weight savings or increase in endurance of about 5%. For commercial flight operations, this improvement is significant because of the potential fuel savings over the life of the vehicle. Even a 1% improvement can be significant. However, in terms of improving military capability, the improvement is probably not significant enough to sell the technology on the basis of gross weight or fuel savings alone. Nevertheless, coupled with the improvement in vehicle control possible with fully adaptive wings given the flexible nature of the wing, the technology may be worth exploring further.

V. Conclusions

This study has addressed the application of large-area aerodynamic control schemes to HALE aircraft systems. In particular, an AFRL joined-wing design is considered, and the benefit of these concepts are determined with respect to performance requirements for two mission segments. It is shown that the roll requirement at landing at positive angle of attack cannot be met by twist actuation alone, but can be met through a combination of twist and camber in an AAW configuration, thus reducing the complications associated with attempting a nose-down landing. At cruise, adaptive structures can be used to optimize camber and twist as the vehicle burns fuel, increasing L/D and reducing fuel requirements, bringing about either increased endurance for constant TOGW, or lower TOGW for constant endurance. Both applications require extensive study before realistic implementation can be considered, but this study has demonstrated that the performance payoff may indeed be worth the investment.

References

[1]Hall, J. M., "Executive Summary AFTI/F-111 Mission Adaptive Wing," Wright Research Development Center, Rept. WRDC-TR-89-2083, Wright–Patterson AFB, OH, Sept. 1989.

[2]Pendleton, E. W., Bessette, D., Field, P. B., Miller, G. D., and Griffin, K. E., "Active Aeroelastic Wing Flight Research Program: Technical Program and Model Analytical Development," *Journal of Aircraft*, Vol. 37, No. 4, 2000, pp. 554–561.

[3]Kudva, J. N., Sanders, B., Pinkerton-Florance, J., and Garcia, E., "The DARPA/AFRL/NASA Smart Wing Program–Final Overview," *Proceedings of the SPIE Smart Structures and Materials Conference: Industrial and Commercial Applications of Smart Structures Technologies*, International Society for Optical Engineering (SPIE), Vol. 4698, July 2002, pp. 37–43.

[4]Lu, K.-J., and Kota, S., "Design of Compliant Mechanisms for Morphing Structural Shapes," *Journal of Intelligent Material Systems and Structures*, Vol. 14, No. 6, 2003, pp. 379–391.

[5]Sultan, C., and Skelton, R. E., "Tendon Control Deployment of Tensegrity Structures," *Proceedings of SPIE 5th International Symposium on Smart Structures and Materials*, International Society for Optical Engineering (SPIE), Vol. 3323, July 1998, pp. 455–466.

[6]Williams, R. B., Park, G., Inman, D. J., and Wilkie, W. K., "An Overview of Composite Actuators with Piezoceramic Fibers," *Proceedings of IMAC-XX: A Conference on Structural Dynamics*, International Society for Optical Engineering (SPIE), Vol. 47531, Jan. 2002, pp. 421–427.

[7]Cesnik, C. E. S., and Brown, E. L., "Active Warping Control of a Joined-Wing Airplane Configuration," AIAA Paper 2003-1715, April 2003.

[8]Mrozinski, D. P., Zeh, J. M., Reich, G. W., Carter, D. L., Cord, T. J., and Shenk, B., "Simulation-Based Research and Development Technology Assessment Process," *Proceedings of the SPIE Conference on Enabling Technology for Simulation Science VI*, International Society for Optical Engineering (SPIE), Vol. 4716, July 2002, pp. 286–294.

[9]Blair, M., and Canfield, R., "A Joined-Wing Structural Weight Modeling Study," AIAA Paper 2002-1337, April 2002.

[10]Wolkovitch, J., "Joined Wing: An Overview," *Journal of Aircraft*, Vol. 23, No. 3, 1986, pp. 161–178.

[11]Reich, G. W., Raveh, D., and Zink, P. S., "Application of Active Aeroelastic Wing Technology to a Joined-Wing Sensorcraft," *Journal of Aircraft*, Vol. 41, No. 3, 2004, pp. 594–602; also AIAA Paper 2002-1633, April 2002.

[12]Chen, P. C., Sarhaddi, D., and Liu, D. D., "Development of the Aerodynamic/Aeroservoelastic Models in ASTROS–Vol. 4: ZAERO Theoretical Manual," U.S. Air Force Research Lab., Rept. AFRL-VA-WP-TR-1999-3052, Wright–Patterson AFB, OH, Feb. 1999.

[13]Johnson, E. H., and Venkayya, V. B., "Automated Structural Optimization System (ASTROS)–Vol. 1: Theoretical Manual," U.S. Air Force Wright Aeronautical Lab., Rept. AFWAL TR-88-3028, Wright–Patterson AFB, OH, Dec. 1988.

[14]Schmidt, L. V., *Introduction to Aircraft Flight Dynamics*, AIAA, Reston, VA, 1998, p. 209.

[15]Miller, G. D., "An Active Flexible Wing Multi-Disciplinary Design Optimization Method," AIAA Paper 94-4412, April 1994.

[16]Zink, P. S., Mavris, D. N., and Raveh, D. E., "Maneuver Trim Optimization Techniques for Active Aeroelastic Wings," *Journal of Aircraft*, Vol. 38, No. 6, 2001, pp. 1139–1146.

[17]Flick, P., and Fields, D., "Continuous Moldline Technology," *AFRL Technology Horizons* [online], Vol. 3, No. 4, 2002, URL:http://www.afrlhorizons.com/Briefs/Dec02/VA0203.html [cited 15 Dec. 2003].

[18]Raymer, D. P., *Aircraft Design: A Conceptual Approach*, AIAA, Washington, DC, 1989, p. 102.

[19]Lamar, J. E., "A Vortex-Lattice Method for the Mean Camber Shapes of Trimmed Noncoplanar Planforms with Minimum Induced Drag," NASA TN D-8090, June 1976.

[20]"High Angle of Attack Stability and Control Prediction Methods and Code," U.S. Air Force Wright Lab., Rept. WL-TR-92-3050, Wright–Patterson AFB, OH, Oct. 1992.